

Present-day crustal deformation and slip rate along the southern Sagaing fault in Myanmar by GNSS observation



Tha Zin Htet Tin^{a,e,*}, Takuya Nishimura^b, Manabu Hashimoto^b, Eric O. Lindsey^{c,d}, Lin Thu Aung^c, Saw Myat Min^f, Myo Thant^{e,f}

^a Graduate School of Science, Kyoto University, Kyoto, Japan

^b Disaster Prevention Research Institute, Kyoto University, Kyoto, Japan

^c Earth Observatory of Singapore, Nanyang Technological University, Singapore

^d Department of Earth and Planetary Sciences, University of New Mexico, Albuquerque, United States

^e Department of Geology, University of Yangon, Yangon, Myanmar

^f Myanmar Earthquake Committee, Yangon, Myanmar

ABSTRACT

The Sagaing fault in Myanmar runs through the entire country and is responsible for major earthquakes, yet only its northern half has been studied geodetically to date. We analyzed Global Navigation Satellite System (GNSS) data to estimate crustal deformation along the central and southern parts of the Sagaing fault. We used a 2-dimensional dislocation model to estimate slip rate, locking depth and lateral offset between surface fault trace and downdip edge of the locked fault along the Sagaing (SGs), Meiktila (MTLs) and Bago (BGOs) segments of the fault. The estimated slip rate is 16–24 mm/yr with a locking depth of 10–16 km in our analysis for the central to southern segments, which is deeper than the locking depth of northern segment from previous studies. The slip rate is ~23–24 mm/yr in the central part of the Sagaing fault, while it is probably slower (~16 mm/yr) in the southern part of our study area. The predicted maximum shear strain from the optimal model is shifted from the surface fault trace. If the locked part of the fault connects directly from the deeper offset dislocation to the surface fault trace, it may be dipping with inferred values of 71°E for the SGs and 78°W for the MTLs, based on the distance between surface trace and the dislocation line at depth. The estimated potential magnitude of earthquakes for each segment as of 2021 are $M_w \sim 7.3$ in SGs, $M_w \sim 7.4$ in MTLs and $M_w \sim 7.3$ in BGOs, respectively.

1. Introduction

Myanmar is situated in an active tectonic region between three major plates: India, Eurasia and Sunda plates (Argus et al., 2011). The India-Sunda oblique convergence is responsible for the formation of the Burma micro-plate which is located between two active plate boundaries: the north-south trending right lateral strike slip Sagaing fault to the east and the Indo-Burmese wedge to the west (Curry et al., 1979; Le Dain et al., 1984; Lin Thu Aung et al., 2019; Steckler et al., 2016; Wang et al., 2014). The oblique subduction is considered to partly contribute to the termination of the 2004 earthquake rupture north of the Andaman Islands (Gahalaut and Gahalaut, 2007). Previous geodetic studies confirmed that the Sunda plate is currently moving eastward with respect to the Eurasia plate (Bock et al., 2003; Chamot-rooke and Le Pichon, 1999; Michel et al., 2001; Simons et al., 1999). The relative motion between the India-Sunda plate is 35 mm/yr in ITRF 2000 at N10° in Myanmar (Socquet et al., 2006) and is considered to be partitioned between the Sagaing fault and Andaman-Arakan Trench (Le Dain et al., 1984; Michel et al., 2001; Peltzer and Saucier, 1996; Tapponnier et al.,

1982; Curry, 1989; Mitchell, 1993). The India and Burma plates are converging at ~12–24 mm/yr across the Indo-Burma Ranges (hereafter IBR) with kinematic coupling of the plate interface extending to a depth of ~30 km (Mallick et al., 2019).

The Myanmar region is separated into two blocks: the eastern block, which includes the Eastern Highland or Shan plateau that belongs to the Sibumasu terrane (Sevastjanova et al., 2016), and the western block known as the Burma plate which consists of Myanmar Central Basin (hereafter MCB) and Indo-Burma Ranges (IBR) (Mitchell et al., 2010; 2012) as shown in Fig. 1. The Sibumasu terrane comprises the Shan plateau of Myanmar, Northwest Thailand, Peninsular Burma and Thailand, western Malaysia and Sumatra and possibly extends northward into western China and Tibet (Metcalfe, 1984).

The Shan plateau is mostly composed of Paleozoic and continental Mesozoic sedimentary rocks with an average elevation of about 1000 m, which occupies most of the eastern part of Myanmar and extends as far as Thailand to the east (Bertrand and Rangin, 2003). It is considered the western edge of the rigid Sundaland block (Vigny et al., 2003). MCB is composed of upper Cretaceous to Pleistocene fluvial sediments that are

* Corresponding author at: E220, Main building, Uji campus, Kyoto University, Gokasho, Uji, Kyoto 611-0011, Japan.

E-mail addresses: tha.tin.44a@st.kyoto-u.ac.jp, thazinhettin@gmail.com (Tha Zin Htet Tin).

locally covered by Quaternary volcanoes (Lin Thu Aung et al., 2020; Pivnik et al., 1998; Mitchell et al., 2010). The Shan scarp is marked as a topographic boundary between the MCB and the Shan plateau or Eastern Highlands (Bertrand and Rangin, 2003). IBR is an active fold and thrust belt composed of schists, pillow lavas, ultramafic rocks, and Triassic to Eocene sedimentary rocks (Sevastjanova et al., 2016).

The Sagaing fault is a major right-lateral strike-slip fault extending over 1200 km, which is connected with the Andaman spreading center at its southern termination (Bertrand and Rangin, 2003). This termination, connected with active seafloor spreading in the Andaman rift (Chamot Cooke et al., 2001; Kamesh Raju et al., 2004) provides a minimum age for the Sagaing fault of 4.5 Ma. The fault is regarded as the western margin of Sundaland and the eastern margin of the Neogene Burma plate. The Burma plate is a forearc sliver which occupies much of western Myanmar, is partially coupled to the Indian plate along the Arakan Trench and is bounded by active tectonic structures (Curray et al., 1979). There are several historical earthquakes along the Sagaing fault. A recent significant earthquake is the M_w 6.8 Thabeikkyin earthquake on 11 November 2012, which claimed 26 fatalities, 12 missing, and injured 231 (Soe Thura Tun and Watkinson, 2017; Seed Asia, 2012). Hurukawa and Maung (2011) pointed out two seismic gaps along the

Sagaing fault between $\sim 19.2^\circ\text{N}$ to $\sim 21.5^\circ\text{N}$ (~ 260 km, $M \sim 7.9$ expected) in central Myanmar and from $\sim 16.6^\circ\text{N}$ to the south (exceeds ~ 180 km, $M \sim 7.7$ or larger earthquake expected) in the Andaman Sea as shown in Fig. 2.

Several authors estimated slip rate along the Sagaing fault using geological, geodetic, and seismological data. Geodetic studies found a slip rate along the central segment of the Sagaing fault of ~ 18 mm/year (Vigny et al., 2003), ~ 22 mm/yr (Maurin et al., 2010), ~ 20 mm/yr (Panda et al., 2018), and ~ 24 mm/yr (Mallick et al., 2019), and ~ 20 mm/yr along the northern segment (Maurin et al., 2010) as shown in Fig. 2. The previous studies proposed to extend Global Navigation Satellite System (GNSS) networks to the western side of MCB and southern part of the Sagaing fault to better constrain a deformation pattern.

Recently, new GNSS networks have been established for continuous stations in 2011 and repeated measurements have been made for campaign stations since 2016. Utilizing new data from continuous sites and campaign surveys of these networks, we analyze the distribution of crustal deformation along the southern segments of the Sagaing fault in more detail. The aim of this study is to estimate present-day relative motion between two blocks along the central and southern segments of the Sagaing fault in Myanmar, and to determine its slip rate, locking

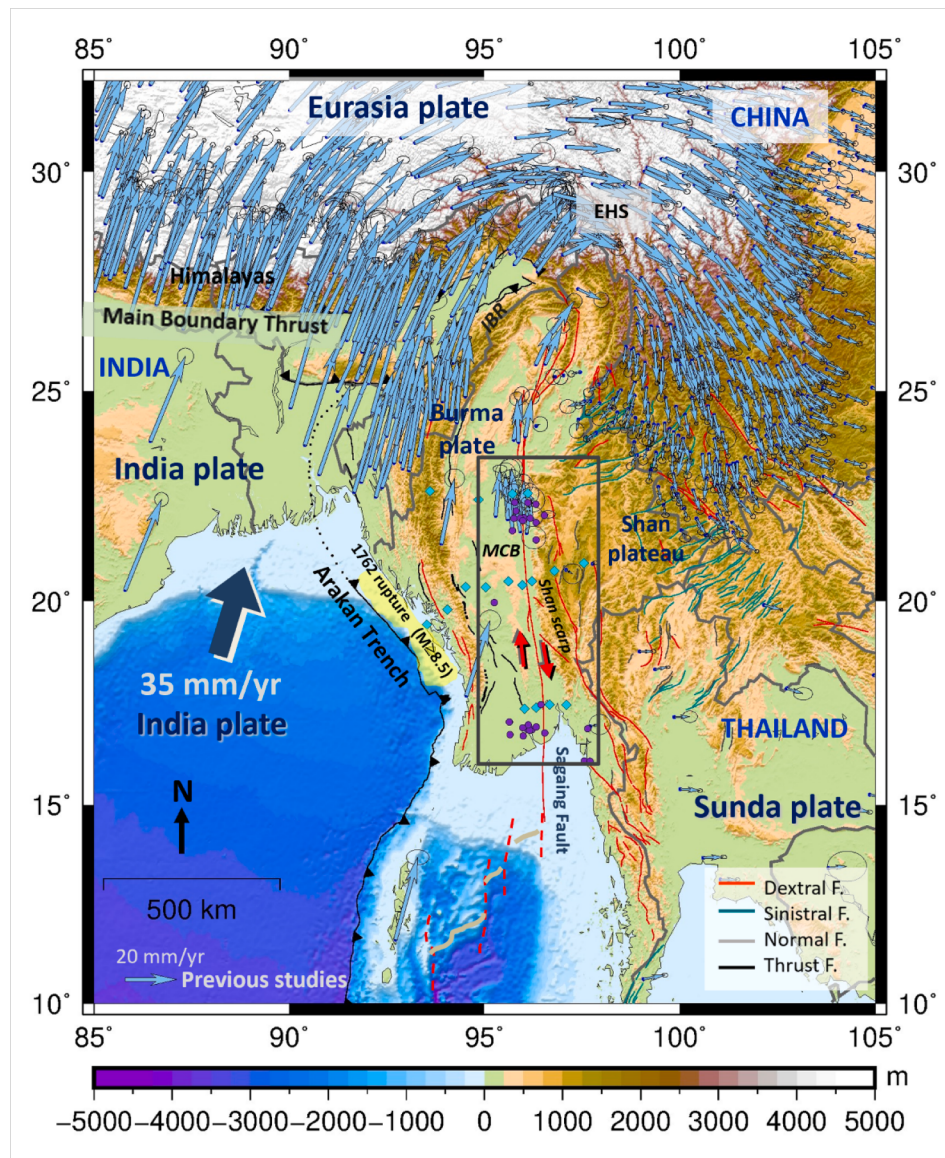


Fig. 1. Regional tectonics and study area in this research. Blue vectors are velocities of GNSS sites with respect to the Eurasia plate and error ellipse show 95% confidence interval (Wang and Shen, 2020). The gray rectangle denotes the study area. Cyan diamonds denote continuous stations of 3 transects perpendicular to the Sagaing fault. Purple dots show the campaign stations. Topographic data is ETOPO1. EHS, Eastern Himalayan Syntaxis; IBR, Indo Burma Ranges; MCB, Myanmar Central Basin.

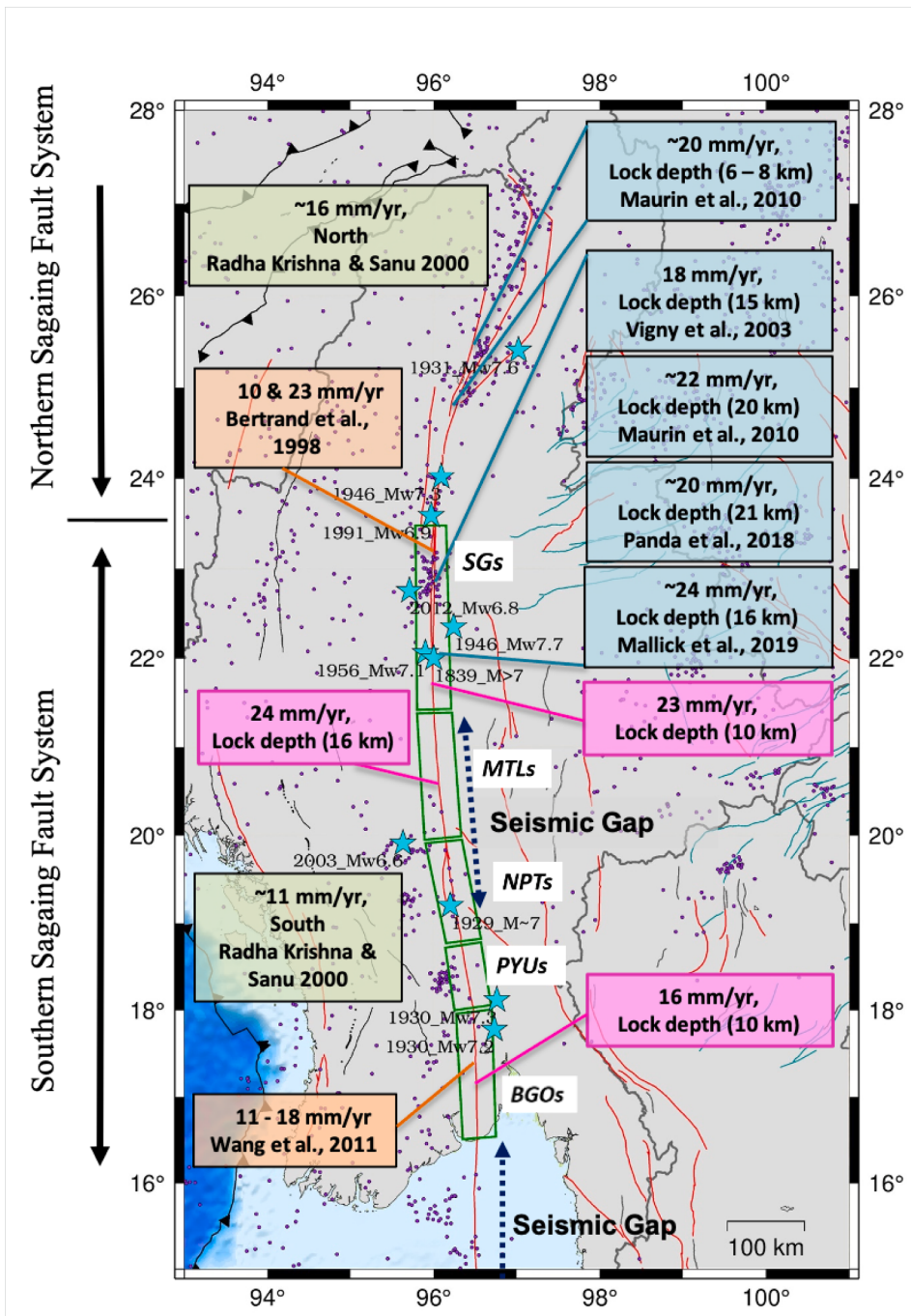


Fig. 2. Slip rates and locking depths along the Sagaing fault in previous studies and this study. Light blue stars denote locations of major earthquakes relocated by Hurukawa and Maung (2011) and Wang et al. (2014). Purple dots denote epicenter of earthquakes with $M \geq 3$ and depth ≤ 40 km during 1908–2020 from the USGS earthquake catalog. Dark blue dash arrows denote seismic gaps from Hurukawa and Maung (2011). Light blue, orange and green text box show slip rates and locking depths estimated in previous studies. Purple text box shows the result in this study. Green rectangles denote segmentation along the southern Sagaing fault system modified after Wang et al. (2014) and Soe Thura Tun and Watkinson (2017). SGs, Sagaing segment; MTLs, Meiktila segment; NPTs, Nay Pyi Taw segment; PYUs, Phyu segment; BGOs, Bago segment.

depth, strain rate distribution and dip angle. Lastly, we aim to clarify the maximum earthquake potential for each segment of the Sagaing fault.

2. Data and methods

A new network consisting of 18 continuous GNSS stations along 3 transects perpendicular to the Sagaing fault from lower to upper Myanmar was constructed under collaboration between the Earth Observatory of Singapore (EOS), Myanmar Earthquake Committee (MEC) and Department of Metrology and Hydrology Myanmar (DMH). The observation of the upper, middle, and lower transects has been in operation since February 2012, November 2017, and November 2011, respectively. Campaign GNSS measurements have been conducted since 2016 to improve coverage along the Sagaing fault in Myanmar. Some

stations around the central Sagaing fault (Mandalay) were repeatedly surveyed in previous studies from Vigny et al. (2003) and Maurin et al. (2010). These sites were also resurveyed during the campaign measurements. We also constructed new concrete monuments (1ft × 1ft and 2 ft deep, metal rod extending 2 ft depth) to densify the network.

In this analysis, we consider only interseismic deformation along the Sagaing fault caused by relative plate motion and exclude the stations which are affected by coseismic and post seismic movements. Coseismic and post seismic motions have affected the continuous stations SDWN and SWBO (near Mandalay area) from the 2012 Thabeikkyin earthquake (Mallick et al., 2019; Pyae Sone Aung et al., 2016) as shown in Fig. 3. We selected the time span for analysis of continuous stations between 2016 and 2019, though data from continuous stations of the middle transect are limited to 2018–2019 because this transect was installed at the end

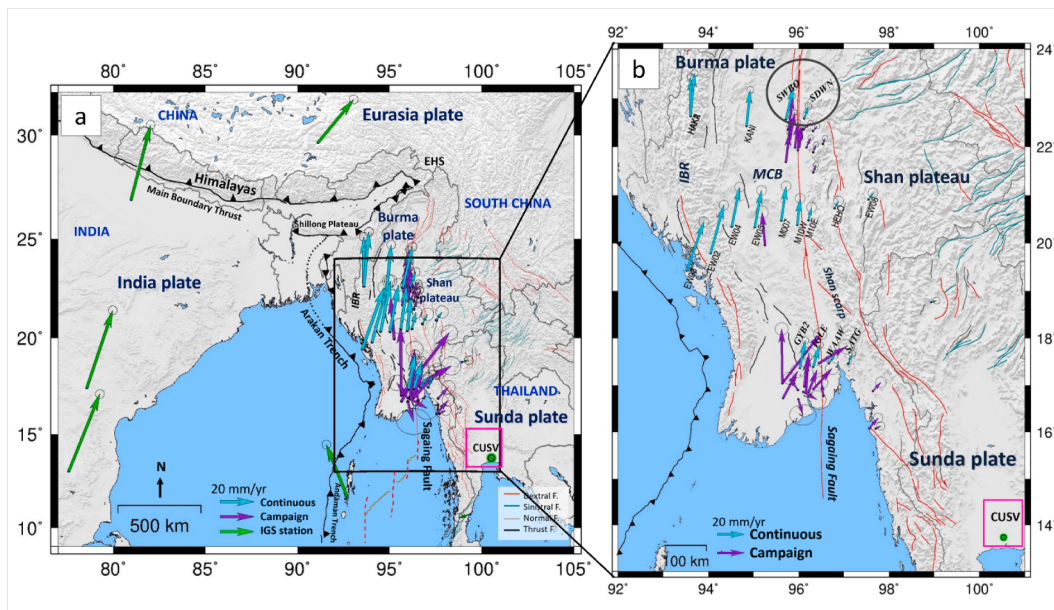


Fig. 3. Velocities of GNSS sites with respect to CUSV station on the Sunda plate. The labels refer to their four-character station ID. (a) Large map view of velocities with respect to CUSV station on the Sunda plate including IGS stations. (b) The closest view of the black rectangle box in (a). All error ellipses show 95% confidence level. Cyan, purple, and green vectors show continuous, campaign and IGS stations velocity vectors, respectively. Pink rectangle boxes denote the reference station. Circle shows the stations (SWBO and SDWN) which are affected by coseismic and postseismic deformation of the 2012 Thabeikkyin earthquake. Detailed description of velocities and uncertainties are given in Table 1. EHS, Eastern Himalayan Syntaxis; IBR, Indo-Burma Ranges; MCB, Myanmar Central Basin.

of 2017. Our surveys of the campaign stations were conducted in 2016, 2017, 2018, and 2019. We also combined previous Receiver Independent Exchange Format (RINEX) data for 13 campaign stations collected by Vigny et al. (2003) and Maurin et al. (2010) in 1998, 2000 and 2005. In total, we analyzed data from 18 continuous stations [8 stations (2016 to 2019 upper and lower transect), 10 stations (2018 to 2019 middle transect and one station from upper transect)] and 29 campaign stations [16 stations (2017, 2018, 2019), 13 stations (1998, 2000, 2005, 2016)] to estimate crustal deformation in Myanmar. We also combined the data from 8 nearby International GNSS Service (IGS) stations (CUSV, LHAZ, HYDE, CPNM, CMUM, LCK4, IISC and PBRI) with a time span of 2016–2019 in our processing and calculated velocities of these stations to fit the whole network to a global reference frame. The detailed description of velocities and surveyed time span is shown in Table 1.

We computed coordinates of both continuous and campaign stations in the International Terrestrial Reference Frame 2014 (ITRF2014) by using GIPSY-OASIS ver 6.4 software with Jet Propulsion Laboratory (JPL) final precise orbits and Precise-Point-Positioning-Ambiguity-Resolution (PPP-AR) strategy (Bertiger et al., 2010). We applied the higher order ionosphere correction and used VMF1 (Boehm et al., 2006) for troposphere mapping correction. Ocean tide loading was calculated using FES2014b model by the Onsala Space Observatory (<http://holt.oso.chalmers.se/loading/>) with respect to the joint mass center of solid Earth and ocean combined in our analysis data (Carrère et al., 2016). We used only horizontal components (EW and NS) of coordinates in the further analysis as shown in Fig. 4. The vertical component (Up and down) includes seasonal variation, hydrological effects, and local site effects (Mallick et al., 2019). Significant deformation occurred at seasonal period with amplitude of vertical displacement about 20 mm (Materna et al., 2021).

We calculated velocities and their uncertainties for both continuous and campaign stations by a least square method applying “stamrg” and “statistics” command in GIPSY. There is both time-uncorrelated (white) and correlated (mostly random-walk) noise in GNSS time series (Langbein and Johnson, 1997). The uncertainties calculated in the GIPSY commands assumed only white noise. Therefore, the random-walk noise would be considered as an additional factor of $R/\sqrt{\text{yr}}$. R is a constant

ranging from 0.5 – 3.3 and the average R is 1.3 (Langbein and Johnson, 1997). We assumed R as average 1.3 and divided by the square root of the observation period in years as $1.3/\sqrt{\text{yr}}$ to determine the random-walk noise contribution. To correct uncertainties between continuous and campaign stations, we calculated realistic uncertainties by assuming sum of white noise and the random-walk noise,

$$\sigma_{\text{real}} = \sqrt{(\sigma_{\text{white}})^2 + (\sigma_{\text{random-walk}})^2}. \quad (1)$$

We subtracted velocity at an IGS station (CUSV), which is in a stable part of the Sunda plate, from estimated velocities to figure out relative motion to CUSV as shown in Fig. 3. The velocity predicted by the rigid rotation of the Sunda plate (Panda et al., 2020) is almost uniform in the studied area, but has a small difference of less than 3 mm/yr due to a rotational component. In the analysis for estimating locking depth, the velocity difference of the rotational component is further smaller (less than 1 mm/yr) in each profile transect of the stations across the Sagaing Fault. Therefore, we simply use the relative velocity to CUSV in the ITRF2014 in this study, although some rotational velocity remains dependent on the rigid motion of the tectonic plate in Fig. 3. Then we divided the southern Sagaing fault into five main segments, i.e., the Sagaing, Meiktila, Nay Pyi Taw, Phy, and Bago segments following previous studies (Wang et al., 2014; Soe Thura Tun and Watkinson, 2017) based on fault geometry, geomorphic expression, and historical seismicity along the southern Sagaing fault. We extended the Sagaing segment by a few km to the south, because our GNSS velocities around there are nearly uniform as shown in Fig. 5a. Therefore, we have ~226 km long Sagaing (21.4°N – 23.5°N) and ~157 km long Meiktila (19.9°N – 21.4°N) segments. Other fault segmentation is similar to previous studies (Wang et al., 2014; Soe Thura Tun and Watkinson, 2017); i.e., ~130 km long Nay Pyi Taw (18.7°N – 19.9°N), ~80 km long Phy (18°N – 18.7°N) and ~162 km long Bago (16.5°N – 18°N) segments.

We fitted the velocity to estimate a downdip depth of a shallow locked (possibly seismogenic) part of the fault (hereafter, a locking depth) and a slip rate at a deep creeping part of the fault (hereafter, a slip rate) by using a 2D dislocation model (Savage and Burford, 1973). We used only the stations which are located within 150 km of the Sagaing fault in order to exclude the velocities which are affected by subduction

Table 1

GNSS sites analyzed in this study.

Site	Longitude	latitude	ITRF 2014		Relative to CUSV in Sunda Plate				Observation Period			
			V _{ew} ^a	V _{ns} ^a	V _{ew} ^a	V _{ns} ^a	σ _{ew}	σ _{ns}				
<i>Fitted stations for locked depth (or 150 km GNSS stations from Sagaing Fault)</i>												
Sagaing Segment												
KANI*	94.8465	22.4340	27.45	17.33	2.67	26.82	1.06	1.06	2016/01–2019/12			
MYOT	95.7161	21.6910	27.44	12.65	2.66	22.14	0.81	0.81	1998/11, 2000/12, 2016/10			
SWBO*	95.7181	22.5724	30.50	14.43	5.71	23.93	1.06	1.06	2016/01–2019/12			
LEGY	95.7567	21.9860	27.35	12.92	2.57	22.41	0.81	0.81	1998/11, 2000/12, 2016/03, 2016/10			
WETL	95.7779	22.3672	27.79	15.13	3.01	24.62	0.81	0.81	1998/11, 2000/12, 2016/11			
THIT	95.8086	22.1618	28.33	10.41	3.54	19.90	0.81	0.81	1998/11, 2000/12, 2016/11			
SAYE	95.9193	21.9913	26.94	9.33	2.16	18.82	0.81	0.81	1998/11, 2000/12, 2005/04, 2016/03, 2016/11			
TNYO	95.9806	21.9340	27.05	7.88	2.26	17.37	0.81	0.81	1998/11, 2000/12, 2016/03, 2016/10			
LEPA	96.0111	22.0031	26.97	5.35	2.19	14.85	0.81	0.81	1998/11, 2000/12, 2016/03, 2016/10			
BODA	96.1108	22.3598	29.91	-4.63	5.13	4.86	0.81	0.81	1998/11, 2000/12, 2016/10			
SDWN*	96.1190	22.5864	28.03	-0.47	3.25	9.02	1.06	1.06	2016/01–2019/12			
YANG	96.1719	21.9892	27.95	-2.11	3.16	7.39	0.81	0.81	1998/11, 2000/12, 2005/04, 2016/02, 2016/10			
KINV	96.3229	21.4730	26.74	-3.80	1.95	5.69	0.81	0.81	1998/11, 2000/12, 2016/10			
ZIBI	96.3212	21.8898	26.78	-3.87	2.00	5.63	0.81	0.81	1998/11, 2000/12, 2016/02, 2016/10			
KUNT	96.3173	22.3243	27.91	-5.68	3.12	3.81	0.81	0.81	1998/11, 2000/12, 2016/10			
YWEN	96.5352	22.0596	26.30	-5.10	1.52	4.39	0.81	0.81	1998/11, 2000/12, 2005/04, 2016/10			
Meiktila Segment												
EW05*	95.0281	20.3326	29.78	18.04	5.00	27.54	1.50	1.50	2018/01–2019/12			
0083	95.2534	19.9598	22.56	15.07	-2.23	24.56	1.92	1.94	2017/11, 2018/12			
M007*	95.6165	20.4735	28.24	16.10	3.46	25.59	1.50	1.50	2018/01–2019/12			
M10W*	95.9710	20.3845	26.79	10.16	2.00	19.66	1.50	1.50	2018/01–2019/12			
M10E*	96.2165	20.4787	27.03	0.10	2.25	9.59	1.50	1.50	2018/01–2019/12			
HEHO*	96.7947	20.7260	27.67	-3.87	2.89	5.63	1.50	1.50	2018/01–2019/12			
EW08*	97.5470	20.9113	28.05	-4.65	3.27	4.84	1.50	1.50	2018/01–2019/12			
Bago Segment												
1020	95.6546	16.7297	35.66	10.63	10.88	20.12	2.12	2.01	2018/03, 2019/03			
CP13	95.9830	16.9001	18.45	-0.67	-6.33	8.82	1.97	1.85	2018/03, 2019/03			
GYB2*	96.0261	17.3688	28.82	11.04	4.03	20.53	1.06	1.06	2016/01–2019/12			
YNGN	96.1239	16.9737	27.12	12.47	2.34	21.96	1.38	1.34	2017/01, 2018/03, 2019/04			
SD02	96.1595	16.8389	26.93	19.84	2.15	29.34	2.06	1.91	2017/01, 2018/03			
CP02	96.2173	16.8543	31.24	7.19	6.45	16.69	1.46	1.38	2017/01, 2018/03, 2019/03			
CP09	96.3282	16.9223	38.66	5.81	13.87	15.30	2.06	1.90	2018/03, 2019/03			
IGLE*	96.3222	17.3970	29.65	6.56	4.87	16.05	1.06	1.06	2016/01–2019/12			
1225	96.4484	17.4707	45.39	2.88	20.60	12.37	2.38	2.20	2018/03, 2019/03			
0707	96.5463	16.7735	23.27	0.60	-1.51	10.09	1.99	1.89	2018/03, 2019/03			
WAAW*	96.6672	17.4694	29.34	-3.63	4.55	5.86	1.06	1.06	2016/01–2019/12			
SATG*	97.0969	17.4624	27.67	-2.15	2.89	7.34	1.06	1.06	2016/01–2019/12			
KYA2	97.5604	16.0804	31.53	-1.70	6.75	7.79	1.45	1.45	2017/01, 2019/03			
1629	97.6435	16.8786	30.74	-2.96	5.96	6.53	1.64	1.61	2017/01, 2019/03			
KYAI	97.7039	16.0750	28.62	-7.52	3.83	1.97	1.27	1.26	2017/01, 2019/03			
{1744}	95.6375	17.0430	24.28	31.11	-0.50	40.60	1.99	1.90	2018/03, 2019/03			
{1021}	95.6382	17.0427	53.14	27.30	28.35	36.79	1.99	1.83	2017/01, 2018/03			
{CP12}	95.9930	16.7004	28.13	-21.15	3.35	-11.65	4.06	3.12	2018/03, 2019/03			
{CP01}	96.1002	16.8567	34.95	-15.08	10.16	-5.59	2.81	2.68	2018/03, 2019/03			
<i>Non-fitted stations for locked depth (or > 150 km GNSS stations from Sagaing Fault)</i>												
HAK2*	93.6045	22.6343	24.76	19.63	-0.02	29.12	1.07	1.07	2018/12–2019/12			
HAKA*	93.6045	22.6345	27.76	22.60	2.98	32.10	1.06	1.06	2016/01–2018/12			
EW04*	94.5174	20.3428	30.64	20.15	5.86	29.64	1.50	1.50	2018/01–2019/12			
EW02*	94.0498	19.7899	34.56	26.37	9.77	35.86	1.50	1.50	2018/01–2019/12			
EW03*	93.5224	19.4258	37.62	26.94	12.84	36.43	1.50	1.50	2018/01–2019/12			
IGS stations												
CMUM*	98.9324	18.7609	28.81	-8.36	4.02	1.13	1.06	1.06	2016/01–2019/12			
CPNM*	99.3744	10.7247	18.10	-11.49	-6.68	-2.00	1.06	1.06	2016/01–2019/12			
CUSV*	100.5339	13.7359	24.78	-9.49	0.00	0.00	0.75	0.75	2016/01–2019/12			
HYDE*	78.5509	17.4173	40.09	36.22	15.31	45.71	1.06	1.06	2016/01–2019/12			
IISC*	77.5704	13.0212	43.14	36.13	18.35	45.63	1.06	1.06	2016/01–2019/12			
LCK4*	80.9556	26.9121	36.28	34.52	11.49	44.01	1.06	1.06	2016/01–2019/12			
LHAZ*	91.1040	29.6573	45.95	15.96	21.16	25.45	1.06	1.06	2016/01–2019/12			
PBRI*	92.7121	11.6378	12.29	21.59	-12.49	31.09	1.06	1.06	2016/01–2019/12			

{ } show rejected stations for fitting locking depth and slip rate.

Note: Site name in bold letters refer eastern side of Sagaing Fault stations.

^a Velocities unit are in mm/yr.

* denote continuous stations.

along the Arakan Trench in this analysis. We considered a dipping fault model by introducing a horizontal offset x_0 of the deep dislocation (which may itself be vertical), as we assume that the locked part of the fault plane is extending from the surface trace to the dislocation edge at depth (Lindsey and Fialko, 2013)

$$v(x) = \frac{v_0}{\pi} \tan^{-1} \left(\frac{x - x_0}{D} \right) + c, \quad (2)$$

where $v(x)$ is the fault parallel component of surface velocity, v_0 is the fault slip rate, x is the perpendicular distance from the surface trace of

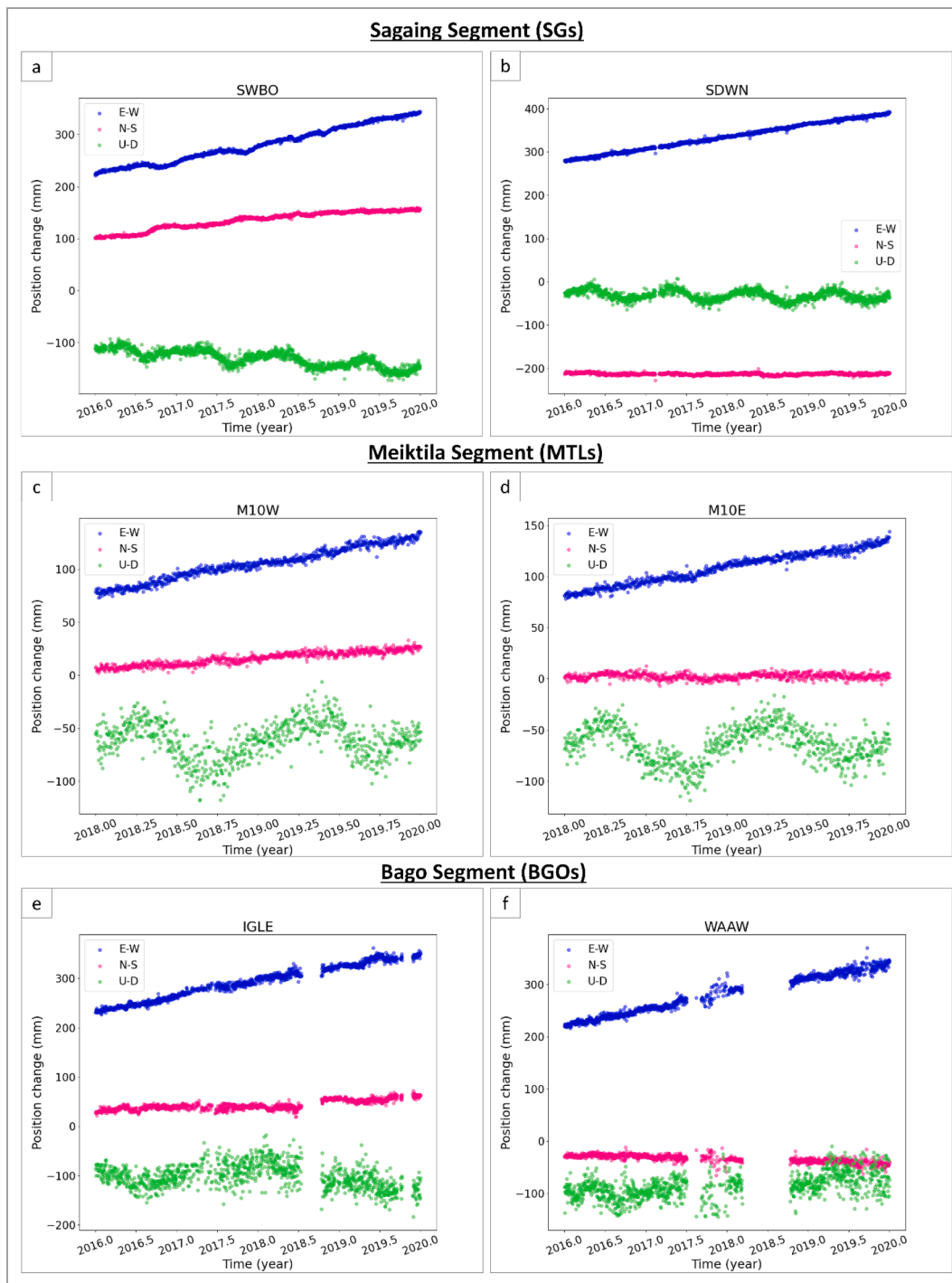


Fig. 4. GNSS time series of selected continuous stations on the eastern and western sides along three segments closest to the Sagaing fault. Station locations are shown in Fig. 3. E-W, N-S, and U-D represent the eastward, northward, and vertical positions, respectively. (a, c and e) Time series of stations on the western side of the Sagaing fault. (b, d and f) Time series of stations on the eastern side of the Sagaing fault.

the fault, x_0 is the offset of the buried dislocation source from the surface trace, D is the locking depth, and c is an unknown DC component mainly due to the motion of the reference point. We used the north component approximately parallel to the fault for fitting of the locking depth and slip rate by minimizing the sum of squared weighted residuals. Velocity uncertainties were used as weight,

$$S(v_0, x_0, D) = \sqrt{\frac{\sum_i^N \frac{(v_i - v(x_i))^2}{\sigma_i^2}}{n}}. \quad (3)$$

We find the optimum locking depth and slip rate that gives the minimum sum of weighted residual divided by the number of fitted stations (n) by changing the locking depth at 1 km interval within the optimal range. We also checked the optimum locking depth and slip rate by using the jackknife resampling method and estimated uncertainties for each segment. In the jackknife resampling method, we find the best optimal values with all free parameters simultaneously by removing one station data for each time calculation in the grid search method. There are 16 samples for the Sagaing segment (SGs), 7 samples for the Meiktila segment (MTLs) and 15 samples for the Bago segment (BGOs)

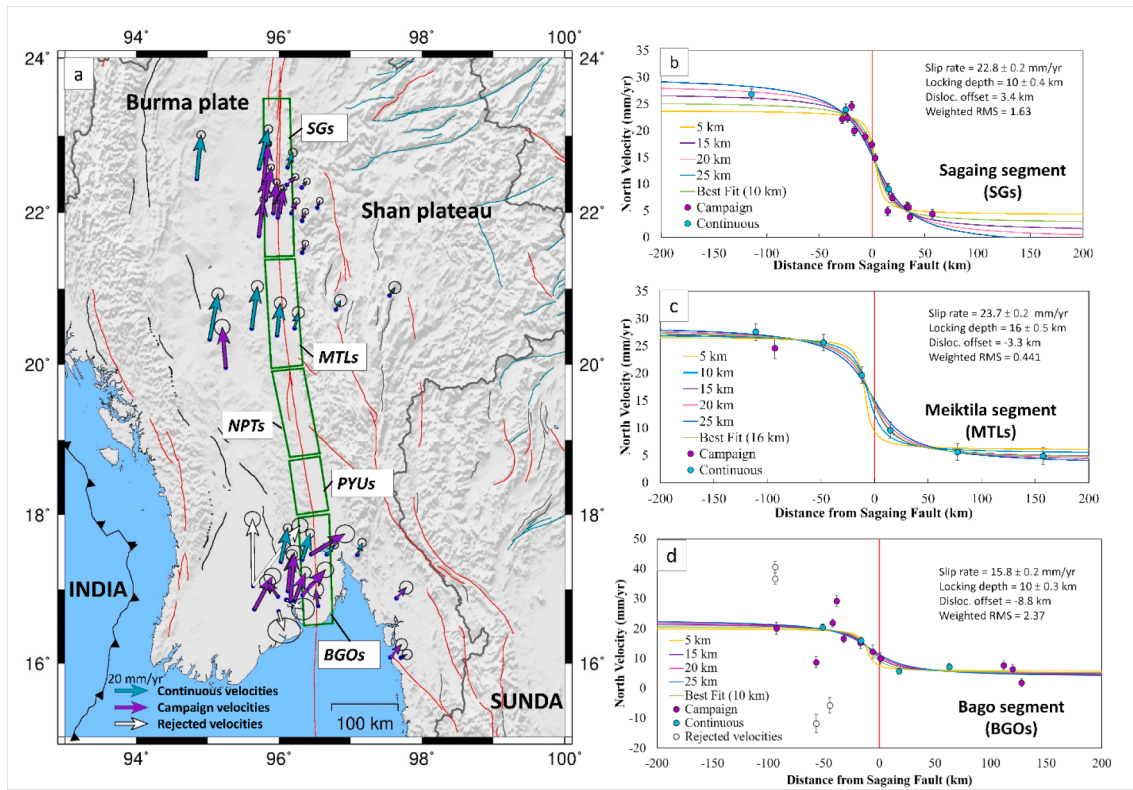


Fig. 5. Estimated slip rate and locking depth. (a) Vectors are observed GNSS velocities within 150 km from the surface trace of the Sagaing fault with respect to CUSV station on the Sunda plate. A station located > 150 km from the fault on the eastern side of the Meiktila segment in a stable land is also included. Cyan and purple vectors indicate the continuous and campaign velocities used in fitting the 2D model and white vectors denote rejected velocities, respectively. Error ellipses show 95% confidence level. SGs, Sagaing segment; MTLs, Meiktila segment; NPTs, Nay Pyi Taw segment; PYUs, Phyuk segment; BGOs, Bago segment. (b, c and d) Observed and calculated fault parallel velocity of 2D dislocation model for 3 segments along the Sagaing fault. Cyan and purple circles denote the velocities fitted to the 2D dislocation model. Open circles denote velocities of rejected stations. Solid colored curves are theoretical profiles for various locking depths at a 5 km interval in Table 2. Green curves denote the theoretical velocities for the optimal model. Error bars denote the uncertainties of the surveyed velocities.

respectively. We calculate the variance and standard deviation for the optimal values of resampled cases at each segment.

Finally, we calculated shear strain distribution by using the equation from Savage and Burford (1973),

$$\epsilon_{xy} = \frac{v_0 D}{2\pi} \frac{1}{(x - x_0)^2 + D^2}. \quad (4)$$

The peak of shear strain shifts either to the eastern or western side of the fault if the locked part of the fault dips. Then we can estimate the dip angle of the locked part of the fault, if we assume a planar fault connecting from the surface trace to the dislocation edge, using locking depth and shift of dislocation source from the surface trace of the fault with the following equation (Lindsey and Fialko, 2013),

$$\theta = \tan^{-1} \frac{D}{x_0}. \quad (5)$$

3. Results

3.1. Estimated velocity field

We subtracted the velocity of the nearby IGS station CUSV which belongs to the stable Sunda plate (Iwakuni et al., 2004). The movement of the GNSS stations are consistent with the dextral strike-slip of the Sagaing fault system as shown in Fig. 3. The motions on the western side might be affected by subduction or the combination of subduction and internal deformation of the Burma plate. The stations located along the subduction trench (>150 km from west of the Sagaing fault) have higher velocities relative to Sunda, up to ~36 mm/yr in fault parallel velocity

(e.g., EW02 and EW03) as shown in Table 1 and Fig. 3. The deformation due to the subduction along the Arakan Trench will require further study to understand deformation in Myanmar. In this study, we used only the stations within ~150 km on each side of the Sagaing fault for estimation of locking depth and slip rate. The 17 stations on the eastern side of the Sagaing fault have significantly smaller velocities than the western side. The estimated velocities on the eastern side for each segment are 4–15 mm/yr (Sagaing segment), 5–10 mm/yr (Meiktila segment) and 2–10 mm/yr (Bago segment). These sites are shown as bold letters in Table 1. The velocities on the western side for each segment are 17–27 mm/yr (Sagaing segment), 20–28 mm/yr (Meiktila segment) and 9–29 mm/yr (Bago segment).

The eastern side of the Sagaing fault is considered a part of the Sunda block in this study, although some internal deformation of the Shan plateau cannot be ruled out. Some estimated velocities on the western side of the Sagaing fault in the Bago segment have significant deviation in direction, which might be related to hydrological effects due to their proximity to populated areas, particularly Yangon city (e.g., van der Horst et al., 2018) and/or survey error on the western side of this segment. We also found seasonal variation in the up and down component of continuous stations as shown in Fig. 4. The other possibility for some campaign stations might be that they are affected by survey error. Therefore, we excluded the campaign stations with the highest and lowest velocities in the Bago segment for the estimation of locking depth and slip rate (Table 1).

3.2. Estimate of slip rate and locking depth

We estimated the locking depth and slip rate for three segments (i.e.,

Table 2

The result of fault parameter inversion along each profile with varying the locking depth.

Description	Locking Depth fixed					Best fit
	Sagaing Segment (SGs)					
Locking Depth (km)	5	10	15	20	25	10
Disloc. offset (km)	3.1	3.4	3.1	2.8	2.8	3.4
slip rate (mm/yr)	19.6	22.8	26.1	29.3	32.4	22.8
Weighted RMS	1.77	1.63	1.73	1.91	2.11	1.63
	Meiktila Segment (MTLs)					
Locking Depth (km)	5	10	15	20	25	16
Disloc. offset (km)	-8.9	-5.9	-3.5	-3	-2.9	-3.3
slip rate (mm/yr)	20.7	22	23.4	24.7	25.9	23.7
Weighted RMS	0.82	0.58	0.444	0.49	0.63	0.441
	Bago Segment (BGOs)					
Locking Depth (km)	5	10	15	20	25	10
Disloc. offset (km)	-10.9	-8.8	-8.6	-8.3	-8.3	-8.8
slip rate (mm/yr)	14.3	15.8	17.1	18.3	19.5	15.8
Weighted RMS	2.41	2.37	2.39	2.44	2.48	2.37

the Sagaing, Meiktila and Bago segments) of the southern Sagaing fault from the obtained velocities. We fitted the 2D dislocation model in Eq. (2) to the fault parallel velocity of the GNSS stations within 150 km on both sides of the Sagaing fault for inversion of each profile. One additional station on the eastern side of the Meiktila segment which shows similar velocity to its neighbors is also included, though it is located slightly farther than 150 km from the fault. First, we fixed the locking depth (D) at 5 km interval according to Maurin et al. (2010) (Fig. 5 and Table. 2) and find the slip rate (v_0) by applying the grid search method with minimizing the weighted RMS. To refine these values, we fixed the locking depth with 1 km interval within the optimal range Fig. 6. We found the optimum locking depth and slip rate that give the minimum weighted root mean square (RMS) residuals (Eq. (3)). The optimal range of locking depth for the Sagaing and Bago segments is between 5 and 15 km, while the Meiktila segment is between 10 and 20 km as shown in Fig. 6. After that, we searched for the optimal values of slip rate and locking depth with all free parameters simultaneously with intervals of 0.1 mm/yr and 0.1 km by applying the grid search method with

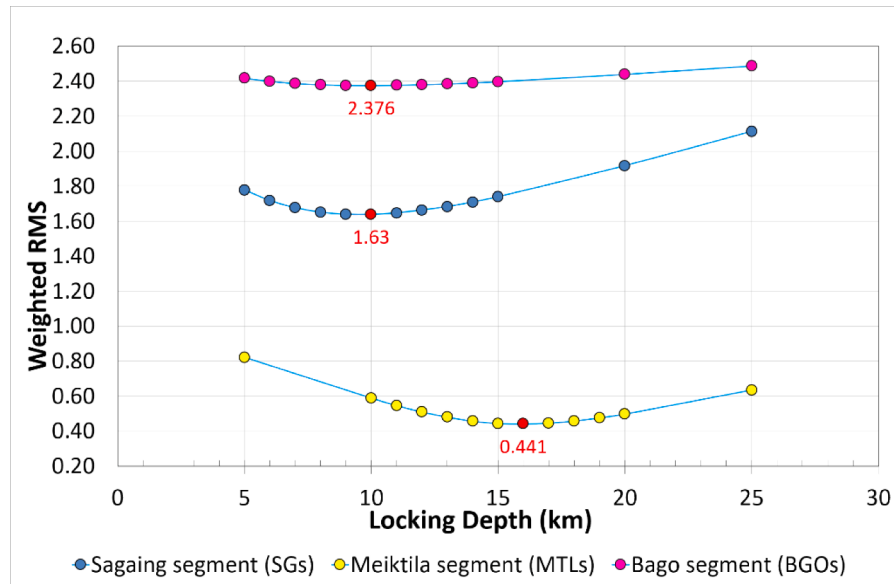


Fig. 6. Weighted RMS distribution for various locking depths. X axis represents the locking depth. Y axis shows the unitless goodness of data fitting defined by Eq. (3).

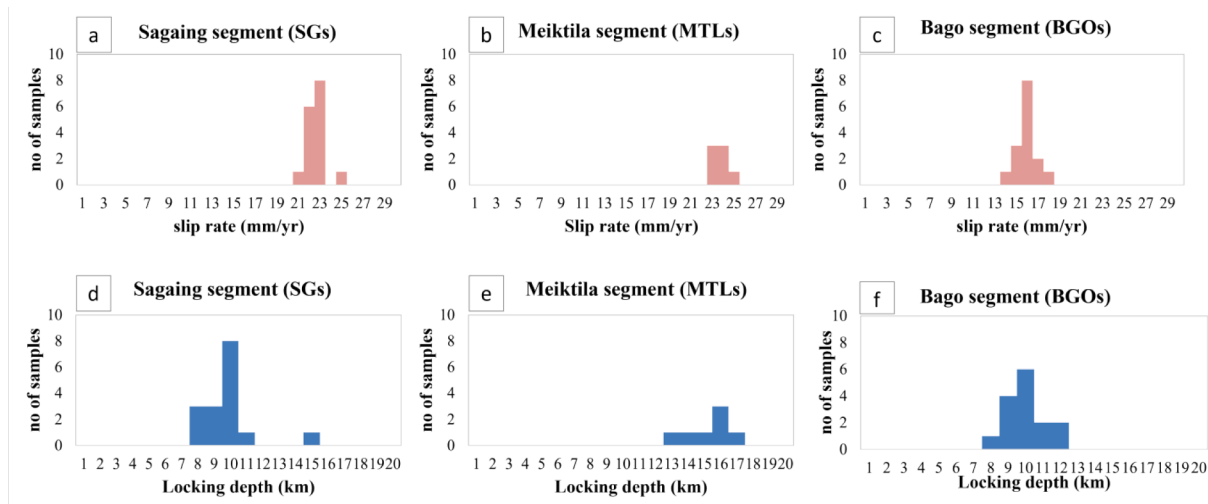


Fig. 7. Histogram of Jackknife analysis for estimation of slip rate and locking depth. (a, b and c) Histograms for estimation of slip rates. (d, e and f) Histograms for estimation of locking depths.

minimizing the weighted RMS.

We also checked the optimum locking depth and slip rate by using the jackknife resampling method with all free parameters and calculated uncertainties for each segment as shown in Fig. 7. The following are the optimum slip rate and the locking depth with uncertainties for each segment.

- (1) Sagaing segment (SGs), 22.8 ± 0.2 mm/yr slip rate and 10 ± 0.4 km locking depth
- (2) Meiktila segment (MTLs), 23.7 ± 0.2 mm/yr slip rate and 16 ± 0.5 km locking depth
- (3) Bago segment (BGOs), 15.8 ± 0.2 mm/yr slip rate and 10 ± 0.3 km locking depth

The estimated slip rate of the GNSS stations along three segments of the southern Sagaing fault ranges from 16–24 mm/yr for this analysis. The velocity of stations in each segment and the optimal 2D dislocation model are shown in Fig. 5. The slip rate is 23–24 mm/yr in the Sagaing (SGs) and Meiktila segments (MTLs). The estimated slip rate is slower in the south, 16 mm/yr in the Bago segment (BGOs). Among these 3 segments, the Meiktila segment is of particular concern as our results suggest a deep locking depth with a high slip rate where there is a lack of historical seismicity in the central part of the Sagaing fault.

3.3. Predicted shear strain distribution and dipping of the fault

We computed shear strain rates along three sections using the estimated slip rates and locking depths. It is obvious that the shear strain is accumulating within 100 km on both sides of the fault as shown in Fig. 8 (a). The highest predicted shear strain rate is $\sim 0.35 \mu\text{strain/yr}$ in the Sagaing segment. This result is probably consistent with the high seismicity around the Sagaing segment, SGs (Figs. 2 and 9). Although we estimate the same locking depth at two segments, the Sagaing (SGs) and Bago (BGOs) segments, the shear strain rate of the BGOs segment is smaller than the SGs due to a lower slip rate. The other possible cause of a high strain rate at the SGs may be the postseismic effect of the 2012

earthquake for this segment. We need to survey existing stations for additional years and analyze any temporal changes in strain rates for this segment. In the Meiktila and Bago segments, the highest predicted shear strain rate is $\sim 0.25 \mu\text{strain/yr}$. Peaks of predicted strain rate for optimal models are shifted ~ 3.4 km to the east of the fault in the Sagaing segment and ~ 3.3 km to the west in the Meiktila segment, while it is shifted ~ 8.8 km to the west of the fault in the Bago segment. There is a possibility that the shallow part of the Sagaing fault is not completely vertical and slightly dipping toward east or the west. Additional geophysical tests are needed to verify this possibility along the Sagaing fault for future study.

We calculated the dip angle for each segment using the offset between the dislocation line and surface trace of the fault and locking depth (Lindsey and Fialko, 2013). It should be noted that the 2D dislocation model for a pure strike-slip fault does not necessarily give dip angle. We referred the surface fault trace as the origin point of the location ($x = 0$). Our interpretation of the dip angle is based on the assumption that the dislocation edge (whether vertical or dipping) is connected by a locked (non-slipping) fault to the surface fault trace at $x = 0$. Thus, we can calculate the dip angle based on the inferred connection between the dislocation edge and the surface fault trace. If the fault is completely vertical, the velocity curve predicted by the dislocation line should be completely symmetrical for both sides. If the fault is dipping east or west, the velocity curve should be asymmetrical with respect to the surface fault trace. We assume that the fault plane extends from the surface trace to the deep dislocation line. Our estimated dip angle is $\sim 71^\circ$ E for the Sagaing segment, $\sim 78^\circ$ W for the Meiktila segment and $\sim 48^\circ$ W for the Bago segment (Fig. 8 (b, c, d) and 9). Chit Thet Mon et al. (2020) pointed out that the earthquakes that occurred along the Sagaing fault (their study area between $\sim 21.4^\circ\text{N}$ to $\sim 23.3^\circ\text{N}$), which is included in the Sagaing segment (SGs), have a maximum focal depth of ~ 26 km with slightly east dipping fault planes.

4. Discussion

In this study, we focus on interseismic deformation along the Sagaing

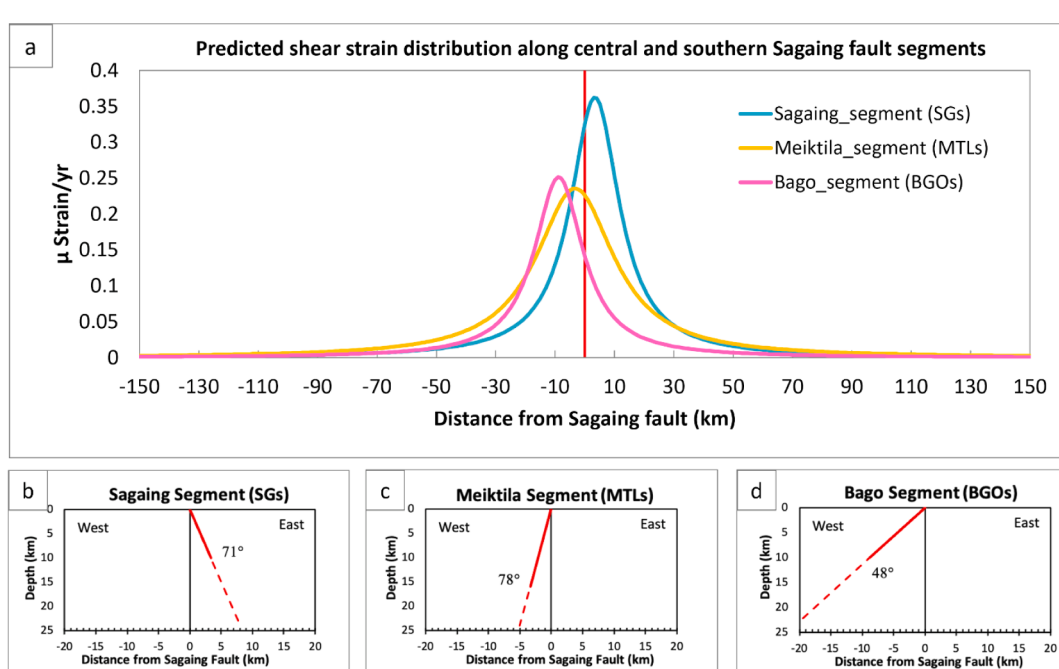


Fig. 8. (a) Predicted maximum shear strain distribution along the Sagaing segment, Meiktila segment and Bago segment. The vertical solid red line denotes the Sagaing fault trace. Blue, orange, and pink curves represent the strain distribution for each segment respectively. (b, c and d) Predicted dip direction along 3 segments of the Sagaing fault. The vertical solid black line denotes the Sagaing fault trace. Solid red line represents the locked part of the fault for each segment. Dashed red line represent the slipping part of the fault extrapolated from the locked part for each segment.

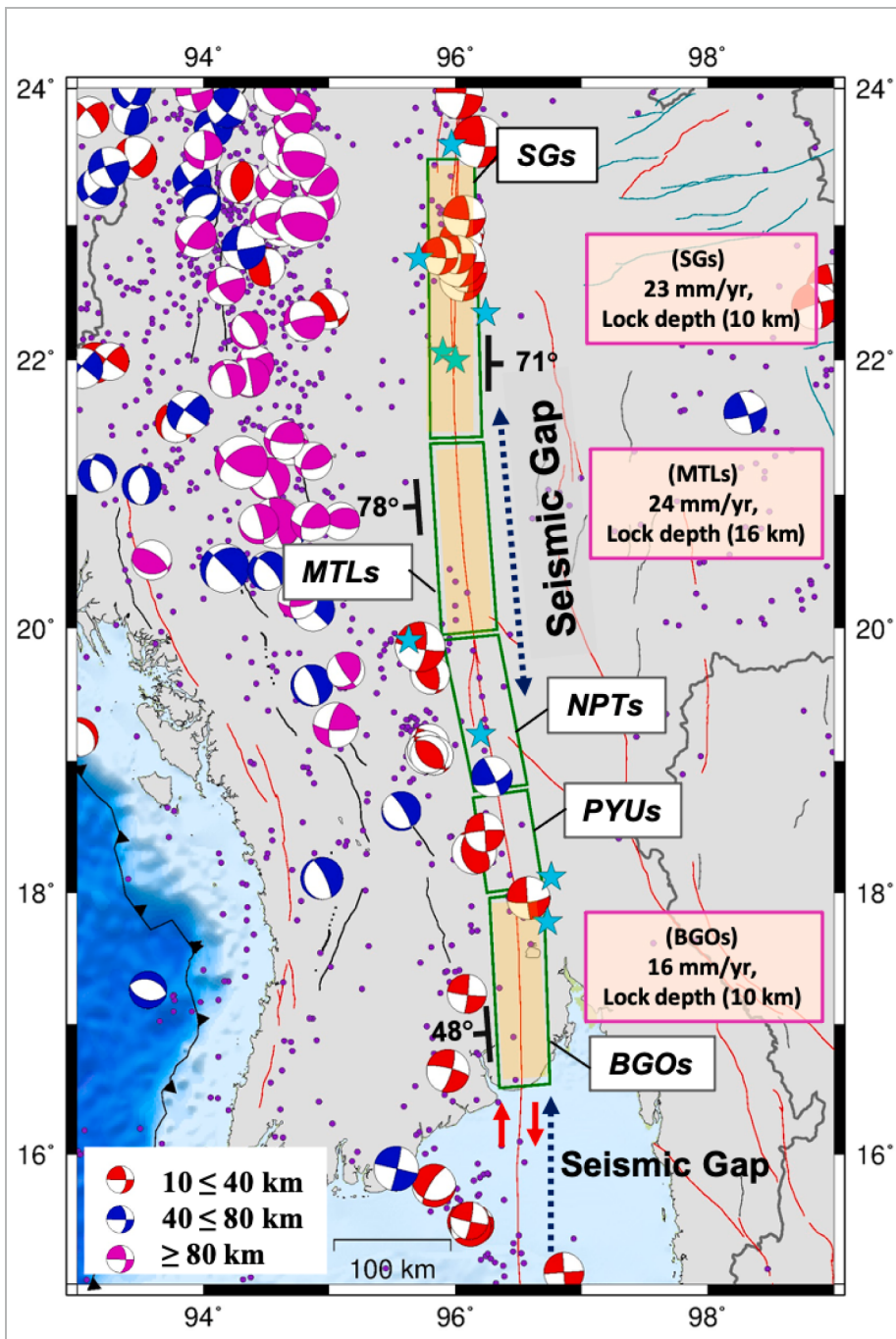


Fig. 9. Predicted dip direction along each segment of the Sagaing fault. Shaded yellow rectangles indicate segments for which dip and slip are estimated. Purple text boxes show slip rate and locking depth for each segment in this study. Light blue stars denote locations of major earthquakes relocated by Hurukawa and Maung (2011) and Wang et al. (2014). Purple dots denote epicenter of earthquakes with $M \geq 3$ and depth ≤ 200 km during 1908–2020 from the USGS earthquake catalog. Focal mechanism is from GCMT reviewed ISC Bulletin $M \geq 5$ (1969–2018). Dark blue dash arrow denotes two seismic gaps from Hurukawa and Maung (2011). SGs, Sagaing segment; MTLs, Meiktila segment; NPTs, Nay Pyi Taw segment; PYUs, Phyu segment; BGOs, Bago segment.

fault due to relative plate motion between the Burma block and the Sunda plate. We excluded the stations which may be affected by earthquakes and subduction along the Arakan Trench. The estimated slip rate in the central part of the Sagaing fault in the previous geodetic studies is between 18 and 20 mm/yr (Vigny et al., 2003), 22 mm/yr (Maurin et al., 2010), 20 mm/yr (Panda et al., 2018) and 24 mm/yr (Mallick et al., 2019). The geological slip rate is estimated to be 10–23 mm/yr based on analysis of offsets of Singu Quaternary basalt using seven samples collected along the central Sagaing fault in the Singu plateau (Bertrand et al., 1998). Wang et al. (2011) estimated a slip rate at the southern end of the Sagaing fault (Bago segment, BGOs) of ~11–18 mm/yr based on radiocarbon dating of charcoal samples. Radha Krishna and Sanu (2000) obtained slip rates of 16 mm/yr (central to north ~480 km [$\sim 21^{\circ}\text{N} - 26^{\circ}\text{N}$]) and 11 mm/yr (central to south ~500

km [$\sim 21^{\circ}\text{N} - 17^{\circ}\text{N}$]) for seismogenic sources along the Sagaing fault by using seismic moment tensors during 1897–1995 shown in Fig. 2.

Our estimated slip rates (16–24 mm/yr) are consistent with the range of geological and geodetic measurement in previous studies, while that from seismic moment tensor summation is a bit smaller. We notice that the southern end of the Sagaing fault has a consistently lower slip rate than that of northern segments in geological, geodetic, and seismic analyses. Possible causes are the interaction of the fault with interseismic coupling along the Arakan Trench, the northward propagation of the Andaman spreading center into the Ayeyarwaddy delta region, southern horse-tail structure of faults in the Andaman spreading center or some other unknown crustal faults on the western side of the Sagaing fault. Further studies are needed to understand the transition of slip rate toward the southern part (Bago segment, BGOs) and we propose

additional survey lines along at least 2 transects consisting of the same number of stations on both the eastern and western sides of the fault like those in the Sagaing and Meiktila segments.

Maurin et al. (2010) estimated a locking depth of 6–8 km in the northern segments of the Sagaing fault. They pointed out that the shallow locking depth might be caused by the existence of creeping sections or the presence of high heat flow from the Tibetan plateau region at the northern end of the Sagaing fault. In the Sagaing segment (SGs), a locking depth is estimated at 15 km by Vigny et al. (2003) and 20 km by Maurin et al. (2010), 21 km by Panda et al. (2018), ~16 km by Mallick et al. (2019), while we obtained 10 km. A strong rheological contrast between two distinct geological domains (Precambrian Shan plateau and Myanmar Central Basin) in the central Sagaing fault may result in a deeper locking depth than the northern segments (Maurin et al. 2010, Panda et al. 2018). The difference between previous studies of locking depth in the Sagaing segment (SGs) may be attributed with the different number of stations and/or may be a result of postseismic deformation from the 2012 earthquake in this segment. Further to the south, the locking depth is 16 km in the Meiktila segment (MTLs) and 10 km in the Bago segment (BGOs) in this study. Our analysis pointed out that the locking depth of the Meiktila segment is deeper than the other two segments as shown in (Figs. 2 and 5).

The peak of shear strain is shifted eastward from the surface trace of the fault in the Sagaing segment (SGs) by 17 km by Vigny et al. (2003), 12 km by Maurin et al. (2010) and 3.4 km in this study. Vigny et al. (2003) suggested that the offset between the fault trace and peak of shear strain might be caused by the activity of the Shan Scarp fault located east of the Sagaing fault, by variations in rheology and thickness of the crust or by a dipping fault plane. However, it is controversial whether the Shan Scarp fault is active or inactive. No seismicity has been detected on the Shan Scarp fault (Myo Thant, 2012) and a recent geological structural map (Soe Thura Tun, 2007) indicates that the Shan Scarp fault is inactive at the present. However, a recent published paper suggested that seismicity may have been detected on the Shan Scarp fault (Chit Thet Mon et al., 2020).

The peak of predicted shear strain rate changes from the east side to the west side of the fault between the Sagaing and Meiktila segments. The Meiktila segment represents a seismic gap pointed out by Hurukawa and Maung (2011), and no historical earthquake is found between these two segments in the USGS earthquake catalog between 1908 and 2020 (Figs. 2 and 9). We applied Kanamori and Anderson (1975) equation and estimated maximum magnitude of the earthquake potential for each segment consideration based on a non-vertical fault. The fault length is assumed as ~226 km for the Sagaing segment (SGs), ~157 km for the Meiktila segment (MTLs) and ~162 km for the Bago segment (BGOs) respectively. We also assume that each segment has accumulated elastic strain since the last large earthquake. The last largest earthquakes happened in 1946 and 1930 in the Sagaing and Bago segments, respectively. The Meiktila segment is assumed to accumulate strain for 100 years because there were no significant historical earthquakes in this segment. If the fault is continuing to accumulate at the current estimated slip rate, the possible potential maximum magnitude as of 2021 is $M_w \sim 7.4$ in the Meiktila segment (MTLs), and $M_w \sim 7.3$ in both the Sagaing segment (SGs) and Bago segment (BGOs) by assuming a 30 GPa shear modulus. Our analysis suggests that the change in dip angle between two segments (SGs and MTLs) might be one mechanism for causing a seismic gap in the central Sagaing fault, with higher strain accumulation and possible potential magnitude in the Meiktila segment (MTLs), with previous ruptures possibly having been halted by the change in fault geometry. It is important to construct additional networks along the Nay Pyi Taw and Phyu segments where no data are currently available, to understand the locking depth in these segments and whether the peak of shear strain rate shifts to the east or west side of the Sagaing fault.

Our estimation of the ~71° E dip angle for the Sagaing segment is consistent with previous studies from seismological data. Tsutsumi and

Sato (2009) pointed out that the Bago segment is close to vertical and remarkably straight based on the observations of the fault trace, which does not coincide with our estimate of shallow west dipping for the Bago segment. Although our estimated dip angle (shallow west dipping ~48° W for Bago segment) may be consistent with the epicentral distribution of earthquakes which are in the western part of the Bago segment (Fig. 2), it is still necessary to obtain additional information by constructing new stations in and around this segment.

The present results are based on an interpretation of the data through 2D dislocation models. There are several sources that affect the GNSS velocity field and add complexities that cannot be explained by the simple 2D dislocation model, such as complex 3D geometry of the fault, crustal heterogeneities etc. We need to examine other geophysical data to verify our suggested gradual ‘twisting’ or ‘changing dip’ of the fault between the Sagaing and Meiktila segments from the Northern to Southern Sagaing fault system, similar to what has been suggested from the San Andreas fault in California, USA (Fuis et al., 2012).

5. Conclusion

We measured crustal deformation along the southern Sagaing fault using continuous and campaign GNSS data collected during the period 2016–2019, together with campaign data from previous studies in 1998, 2000, 2005 near the Mandalay area (central Myanmar), using GIPSY-OASIS ver 6.4 software in ITRF 2014. From the results of the analysis, we derived the following conclusions.

(1) The eastern side of the Sagaing fault (Shan plateau) has a small velocity relative to the site CUSV on stable Sundaland. It suggests that the eastern side of the Sagaing fault belongs to the part of the Sunda plate with little internal deformation. On the other hand, the western side of the Sagaing fault moves northward by up to 30 mm/yr, implying dextral strike-slip of this fault.

(2) We estimated the slip rate of the central and southern Sagaing fault from the GNSS velocities within 150 km on both sides of the fault using a 2D dislocation model. We obtained slip rates of ~20–24 mm/yr in the central part (Sagaing segment (SGs) and Meiktila segment (MTLs)), consistent with earlier geologic and geodetic studies in this area. The slip rate is slower (15–16 mm/yr) along the southern end of the fault (Bago segment). This is consistent with the previous estimate of ~11–18 mm/yr along the Bago segment, though it is presently not clear where the remaining slip budget along the southern section is accommodated.

(3) Optimal locking depths are 10 km for the Sagaing segment, 16 km for the Meiktila segment and 10 km for the Bago segment in our dataset.

(4) The peak of predicted shear strain rate is shifted from the eastern side to the western side along the Sagaing and Meiktila segments, respectively, which suggests the deep dislocation line is offset from the surface trace of the fault. Assuming the locked part of the fault plane is connected to the surface trace, we estimated a dip angle of ~71° E for the Sagaing segment and ~78° W for the Meiktila segment. This change of dip angle between these two segments might affect rupture propagation and could be one of the reasons for the seismic gap in central part of the Sagaing fault.

(5) The estimated potential magnitude of earthquakes for each segment as of 2021 are $M_w \sim 7.4$ in the Meiktila segment (MTLs), $M_w \sim 7.3$ in the Sagaing segment (SGs) and the Bago segment (BGOs).

There is a gap in the present GNSS network along part of the Sagaing fault and we cannot presently estimate parameters for the Nay Pyi Taw and Phyu segments. Additional surveys and analyses are desired to improve our understanding of the characteristics and motion of the Sagaing fault.

CRediT authorship contribution statement

Tha Zin Htet Tin: Conceptualization, Methodology, Investigation, Writing – original draft, Visualization. **Takuya Nishimura:** Software,

Validation, Writing – review & editing, Visualization. **Manabu Hashimoto:** Supervision, Writing – review & editing, Visualization. **Eric O. Lindsey:** Data curation, Resources, Writing – review & editing, Validation. **Lin Thu Aung:** Resources, Writing – review & editing. **Saw Myat Min:** Resources. **Myo Thant:** Resources, Visualization.

Declaration of Competing Interest

The authors declare that they have no known competing financial interests or personal relationships that could have appeared to influence the work reported in this paper.

Acknowledgements

We would like to thank the Earth Observatory of Singapore (EOS), the Myanmar Earthquake Committee (MEC), Department of Metrology and Hydrology, Myanmar (DMH) for kindly sharing their data for this research. We are grateful to Mr. Win Pyae Htet, Mr. Saw Pyae and Mr. Eain Thu (MEC), Mr. Than Khaing (Myanmar Survey Department, MSD), Mr. Pyae Sone Aung (Center for Geohazard Observation, EOS), Prof. Wang Yu (National Taiwan University) and Mr. Oo Than (DMH) for their co-operation in field survey and maintenance of GNSS stations in Myanmar. We would like to express our sincere acknowledgement to anonymous reviewers for their reviews and constructive comments that greatly improved this manuscript. We also thank the IGS, USGS and ISC for sharing GNSS data for reference stations from IGS network and earthquake catalogs. We use GMT version 5.4.3 (Wessel et al., 2013) for making maps. We would like to give special thanks to Mr. Yutaro Okada, Dr. Hiromu Sakaue and Dr. Yuji Itoh who supported and gave help for data analysis in the lab. We also appreciate Prof. Emma M. Hill (Asian School of Environment, EOS) for reading the manuscript and giving helpful suggestions for this work. We express gratitude to Professor Dr. Day Wa Aung, Professor and Head of the Department of Geology, University of Yangon, for kind permission participate in field work for this research project. The first author would like to thank Japan International Cooperation Agency (JICA) for giving a scholarship and support for this research work. Field works and maintenance of the GNSS network for this research were supported by the Earth Observatory of Singapore via its funding from the National Research Foundation of Singapore, and the Singapore Ministry of Education under the Research Centers of Excellence initiative. This work comprises EOS contribution number (423).

References

- Argus, D.F., Gordon, R.G., DeMets, C., 2011. Geologically current motion of 56 plates relative to the no-net-rotation reference frame. *Geochemistry, Geophysics, Geosystems* 12 (11), n/a–n/a. <https://doi.org/10.1029/2011GC003751>.
- Bertiger, W., Desai, S.D., Haines, B., Harvey, N., Moore, A.W., Owen, S., Weiss, J.P., 2010. Single receiver phase ambiguity resolution with GPS data. *J. Geod.* 84 (5), 327–337. <https://doi.org/10.1007/s00190-010-0371-9>.
- Bertrand, G., Rangin, C., 2003. Tectonics of the western margin of the Shan plateau (central Myanmar): Implication for the India-Indochin oblique convergence since the Oligocene. *J. Asian Earth Sci.* 21, 1139–1157. [https://doi.org/10.1016/S1367-9120\(02\)00183-9](https://doi.org/10.1016/S1367-9120(02)00183-9).
- Bertrand, G., Rangin, C., Maury, R.C., Htun, H.M., Bellon, H., Guillaud, J.P., 1998. Les basaltes de Singu (Myanmar): Nouvelles contraintes sur le taux de décrochement récent de la faille de Sagaing. *Comptes Rendus l'Academie Sci. - Ser. IIa Sci. la Terre des Planetes* 327, 479–484. [https://doi.org/10.1016/S1251-8050\(99\)80076-7](https://doi.org/10.1016/S1251-8050(99)80076-7).
- Bock, Y., Prawirodirdjo, L., Genrich, J.F., Stevens, C.W., McCaffrey, R., Subarya, C., Puntodewo, S.S.O., Calais, E., 2003. Crustal motion in Indonesia from Global Positioning System measurements. *J. Geophys. Res.* 108. <https://doi.org/10.1029/2001JB000324>.
- Boehm, J., Werl, B., Schuh, H., 2006. Troposphere mapping functions for GPS and very long baseline interferometry from European Centre for Medium-Range Weather Forecasts operational analysis data: TROPOSPHERE MAPPING FUNCTIONS FROM ECMWF. *J. Geophys. Res.: Solid Earth* 111 (B2), n/a–n/a. <https://doi.org/10.1029/2005JB003629>.
- Carrère L., Lyard, F., Cancet, M., Guillot, A., Picot N., 2016. Finite Element Solution FES2014, a new tidal model - Validation results and perspectives for improvements, presentation to ESA Living Planet Conference, Prague 2016. FES2014.
- Chamot-Rooke, N., Le Pichon, X., 1999. GPS determined eastward Sundaland motion with respect to Eurasia confirmed by earthquakes slip vectors at Sunda and Philippine trenches. *Earth Planet. Sci. Lett.* 173 (4), 439–455.
- Chamot-Rooke, N., Rangin, C., Nielsen, C., 2001. Timing and kinematics of Andaman basin opening. *Eos Trans. Suppl.* 82, 20.
- Chit Thet Mon, Gong, X., Wen, Y., Jiang, M., Chen, Q.F., Zhang, M., Hou, G., Thant, M., Sein, K., He, Y., 2020. Insight Into Major Active Faults in Central Myanmar and the Related Geodynamic Sources. *Geophys. Res. Lett.* 47, 1–8. <https://doi.org/10.1029/2019GL086236>.
- Curry, J.R., Moore, D.R., Lawver, L.A., Emmel, F.J., Waitt, R.W., Hery, M., Kieckhefer, R., 1979. Tectonics of the Andaman Sea and Burma. *AAPG Memoir* 29, 189–198.
- Curry, J.R., 1989. The Sunda Arc: A Model for Oblique Plate Convergence. *Netherlands J. Sea Res.* 24 (2-3), 131–140.
- Fuis, G.S., Scheirer, D.S., Langenheim, V.E., Kohler, M.D., 2012. A new perspective on the Geometry of the San Andreas fault in southern California and its relationship to Lithospheric structure. *Bull. Seismol. Soc. Am.* 102 (1), 236–251. <https://doi.org/10.1785/0120110041>.
- Gahalaut, V.K., Gahalaut, K., 2007. Burma plate motion 112, 1–9. <https://doi.org/10.1029/2007JB004928>.
- van der Horst, T., Rutten, M.M., van de Giesen, N.C., Hanssen, R.F., 2018. Remote Sensing of Environment Monitoring land subsidence in Yangon, Myanmar using Sentinel-1 persistent scatterer interferometry and assessment of driving mechanisms. *Remote Sens. Environ.* 217, 101–110. <https://doi.org/10.1016/j.rse.2018.08.004>.
- Hurukawa, N., Maung Maung, P., 2011. Two seismic gaps on the Sagaing Fault, Myanmar, derived from relocation of historical earthquakes since 1918. *Geophys. Res. Lett.* 38 (1), n/a–n/a. <https://doi.org/10.1029/2010GL046099>.
- Iwakuni, M., Kato, T., Takiguchi, H., Nakagawa, T., Satomura, M., 2004. Crustal deformation in Thailand and tectonics of Indochina peninsula as seen from GPS observations. *Geophys. Res. Lett.* 31 (11), n/a–n/a. <https://doi.org/10.1029/2004GL020347>.
- Kanamori, H., Anderson, D.L., 1975. Theoretical basis of some empirical relations in seismology by. *Bull. Seismol. Soc. Am.* 65, 1073–1095.
- Radha Krishna, M., Sanu, T.D., 2000. Seismotectonics and rates of active crustal deformation in the Burmese arc and adjacent regions. *J. Geodyn.* 30 (4), 401–421. [https://doi.org/10.1016/S0264-3707\(99\)00074-5](https://doi.org/10.1016/S0264-3707(99)00074-5).
- Langbein, J., Johnson, H., 1997. Correlated errors in geodetic time series: Implications for time-dependent deformation. *J. Geophys. Res. B Solid Earth* 102 (B1), 591–603.
- Le Dain, A.Y., Tapponnier, P., Molnar, P., 1984. Active Faulting and Tectonics of Burma and Surrounding Regions. *J. Geophys. Res.* 89 (B1), 453. <https://doi.org/10.1029/JB089B01p00453>.
- Lin Thu Aung, Martin, S.S., Wang, Y., Wei, S., Thant, M., Htay, K.N., Aung, H.M., Kyaw, T.Z., Min, S., Sithu, K., Naing, T., Khaing, S.N., Oo, K.M., Suresh, G., Chen, W., Maung, P.M., Gahalaut, V., 2019. Tectonophysics A comprehensive assessment of ground motions from two 2016 intra-slab earthquakes in Myanmar. *Tectonophysics* 765, 146–160. <https://doi.org/10.1016/j.tecto.2019.04.016>.
- Lin Thu Aung, Oo, K.Z., Win, K.M., Moore, G.F., Tun, S.T., Naing, W., 2020. Active deformation of the Central Myanmar Forearc Basin: Insight from post-Pleistocene inversion of the Pyay Fault. *J. Asian Earth Sci.* X 4, 100037. <https://doi.org/10.1016/j.jaexs.2020.100037>.
- Lindsey, E.O., Fialko, Y., 2013. Geodetic slip rates in the southern San Andreas Fault system: Effects of elastic heterogeneity and fault geometry. *J. Geophys. Res. Solid Earth* 118 (2), 689–697. <https://doi.org/10.1029/2012JB009358>.
- Mallick, R., Lindsey, E.O., Feng, L., Hubbard, J., Banerjee, P., Hill, E.M., 2019. Active Convergence of the India-Burma-Sunda Plates Revealed by a New Continuous GPS Network. *J. Geophys. Res. Solid Earth* 124 (3), 3155–3171. <https://doi.org/10.1029/2018JB016480>.
- Materna, K., Feng, L., Lindsey, E.O., Hill, E.M., Ahsan, A., Alam, A.K.M.K., Oo, K.M., Than, O., Aung, T., Khaing, S.N., Bürgmann, R., 2021. GNSS characterization of hydrological loading in South and Southeast Asia. *Geophys. J. Int.* 224, 1742–1752. <https://doi.org/10.1093/gji/gjaaf500>.
- Maurin, T., Masson, F., Rangin, C., Min, U.T., Collard, P., 2010. First global positioning system results in northern Myanmar: Constant and localized slip rate along the Sagaing fault. *Geology* 38 (7), 591–594. <https://doi.org/10.1130/G30872.110.110.2010162>.
- Metcalfe, I., 1984. Stratigraphy, palaeontology and palaeogeography of the Carboniferous of Southeast Asia. *Mem. Soc. Geol. France* 147, 107–118.
- Michel, G.W., Yu, Y.Q., Zhu, S.Y., Reigner, C., Becker, M., Reinhart, E., Simons, W., Ambrosius, B., Vigny, C., Chamot-Rooke, N., Le Pichon, X., Morgan, P., Matheussen, S., 2001. Crustal motion and block behaviour in SE-Asia from GPS measurements. *Earth Planet. Sci. Lett.* 187 (3-4), 239–244.
- Mitchell, A.H.G., 1993. Cretaceous-Cenozoic tectonic events in the western Myanmar (Burma). *-Assam region* 150 (6), 1089–1102.
- Mitchell, A.H.G., Hlaing, T., Htay, N., 2010. The chin hills segment of the Indo-Burman ranges: not a simple accretionary wedge. In: Ibotombi, S. (Ed.), Indo-Myanmar ranges in the tectonic framework of the Himalaya and Southeast Asia. Geological Society of India, Memoir 75. Bangalore, pp. 3–24.
- Mitchell, A., Chung, S., Oo, T., Lin, T., Hung, C., 2012. Journal of Asian Earth Sciences Zircon U–Pb ages in Myanmar: Magmatic–metamorphic events and the closure of a neo-Tethys ocean? *J. Asian Earth Sci.* 56, 1–23. <https://doi.org/10.1016/j.jseas.2012.04.019>.
- Myo Thant, 2012. Seismic hazard assessment for Myanmar. *Myanmar Earthquake Committee and Myanmar Geoscience Society, Yangon, Myanmar*.
- Panda, D., Kundu, B., Gahalaut, V.K., Rangin, C., 2018. Crustal deformation, spatial distribution of earthquakes and along strike segmentation of the Sagaing Fault,

- Myanmar. J. Asian Earth Sci. 166, 89–94. <https://doi.org/10.1016/j.jseaes.2018.07.029>.
- Panda, D., Kundu, B., Gahalaut, V.K., Rangin, C., 2020. India-Sunda Plate Motion, Crustal Deformation, and Seismic Hazard in the Indo-Burman Arc. *Tectonics* 39 (8). <https://doi.org/10.1029/2019TC006034>.
- Peltzer, G., Saucier, F., 1996. Present-day kinematics of Asia derived from geologic fault rates. *J. Geophys. Res.* 10, 27943–27956.
- Pivnik, D.A., Nahm, J., Tucker, R.S., Smith, G.O., Nyein, K., Nyunt, M., Maung, P.H., 1998. Polyphase deformation in a fore-arc/back-arc basin, Salin Subbasin, Myanmar (Burma). *AAPG Bull.* 82, 1837–1856.
- Pyae Sone Aung, Satirapod, C., Andrei, C.-O., 2016. Sagaing Fault slip and deformation in Myanmar observed by continuous GPS measurements. *Geod. Geodyn.* 7 (1), 56–63. <https://doi.org/10.1016/j.geog.2016.03.007>.
- Kamesh Raju, K.A., Ramprasad, T., Rao, P.S., Ramalingeswara Rao, B., Varghese, J., 2004. New insights into the tectonic evolution of the Andaman basin. *Northeast Indian Ocean* 221 (1-4), 145–162. [https://doi.org/10.1016/S0012-821X\(04\)00075-5](https://doi.org/10.1016/S0012-821X(04)00075-5).
- Savage, J.C., Burford, R.O., 1973. Geodetic determination of relative plate motion in central California. *J. Geophys. Res.* 78 (5), 832–845.
- Sevastjanova, I., Hall, R., Rittner, M., Mu, S., Lay, T., Tin, T., Alderton, D.H., Comfort, G., 2016. Myanmar and Asia united, Australia left behind long ago. *Gondwana Res.* 32, 24–40. <https://doi.org/10.1016/j.gr.2015.02.001>.
- Simons, W.J.F., Ambrosius, B.A.C., Noomen, R., Angermann, D., Vigny, C., 1999. Observing Plate Motions in S. E. Asia: Geodetic results of the GEODYSSSEA project. *Geophys. Res. Lett.* 26, 2081–2084.
- Socquet, A., Vigny, C., Chamot-Rooke, N., Simons, W., Rangin, C., Ambrosius, B., 2006. India and Sunda plates motion and deformation along their boundary in Myanmar determined by GPS. *J. Geophys. Res. Solid Earth* 111 (B5), n/a–n/a. <https://doi.org/10.1029/2005JB003877>.
- Seed Asia 2012. The 2012 Thabeikkyin Earthquake SEEDS Asia, 1–28. Retrieved from www.seedasia.org.
- Soe Thura Tun, 2007. Tectonic Map of Myanmar and Surrounding Regions. 1:2,000,000 scale. Myanmar Geoscience Society, Yangon, Myanmar.
- Soe Thura Tun, Watkinson, I.M., 2017. The Sagaing Fault, Myanmar. *Geol. Soc. Mem.* 48, 413–441. <https://doi.org/10.1144/M48.19>.
- Steckler, M.S., Mondal, D.R., Akhter, S.H., Seeber, L., Feng, L., Gale, J., Hill, E.M., Howe, M., 2016. Locked and loading megathrust linked to active subduction beneath the Indo-Burman Ranges. *Nat. Geosci.* 9 (8), 615–618. <https://doi.org/10.1038/geo2760>.
- Tapponnier, P., Peltzer, G., Dain, A.Y. Le, Armijo, R., Jussieu, P., Cobbold, P., 1982. Propagating extrusion tectonics in Asia : New insights from simple experiments with plasticine 611–616.
- Tsutsumi, H., Sato, T., 2009. Tectonic Geomorphology of the Southernmost Sagaing Fault and Surface Rupture Associated with the May 1930 Pegu (Bago) Earthquake. *Myanmar* 99 (4), 2155–2168. <https://doi.org/10.1785/0120080113>.
- Vigny, C., Socquet, A., Rangin, C., Chamot-Rooke, N., Pubellier, M., Bouin, M.-N., Bertrand, G., Becker, M., 2003. Present-day crustal deformation around Sagaing. *J. Geophys. Res.* 108. <https://doi.org/10.1029/2002jb001999>.
- Wang, M., Shen, Z.-K., 2020. Present-Day Crustal Deformation of Continental China Derived From GPS and Its Tectonic Implications. *J. Geophys. Res. Solid Earth* 125 (2). <https://doi.org/10.1029/2019JB018774>.
- Wang, Y., Sieh, K., Aung, T., Min, S., Khaing, S.N., Tun, S.T., 2011. Earthquakes and slip rate of the southern Sagaing fault: Insights from an offset ancient fort wall, lower Burma (Myanmar). *Geophys. J. Int.* 185, 49–64. <https://doi.org/10.1111/j.1365-246X.2010.04918.x>.
- Wang, Y.U., Sieh, K., Tun, S.T., Lai, K.-Y., Myint, T., 2014. Active tectonics and earthquake potential of the Myanmar region. *J. Geophys. Res. Solid Earth* 119 (4), 3767–3822. <https://doi.org/10.1002/2013JB010762>.
- Wessel, P., Smith, W.H.F., Scharroo, R., Luis, J., Wobbe, F., 2013. Generic mapping tools: Improved version released. *Eos (Washington, DC)* 94 (45), 409–410. <https://doi.org/10.1002/2013EO450001>.